Bull. Mater. Sci., Vol. 40, No. 3, June 2017, pp. 435–439
DOI 10.1007/s12034-017-1391-3

SU-8 photoresist-derived electrospun carbon nanofibres as high-capacity anode material for lithium ion battery

M KAKUNURI, S KAUSHIK, A SAINI and C S SHARMA*
Creative and Advanced Research Based On Nanomaterials (CARBON) Laboratory, Department of Chemical Engineering, Indian Institute of Technology, Hyderabad, Kandi 502285, India
*Author for correspondence (cssharma@iith.ac.in)

MS received 5 May 2016; accepted 22 July 2016; published online 9 June 2017

Abstract. A binder-free carbon nanofibres web over stainless-steel wafer current collector was fabricated by controlled pyrolysis of electrospun SU-8 photoresist nanofibres. Electrochemical performance of the as-prepared carbon nanofibres web was investigated by performing charge–discharge experiments at different current densities. At low current density (37.2 mA g^{-1}, 0.1C), SU-8-derived carbon nanofabric showed a large initial discharge capacity (1417 mAh g^{-1}) with sufficiently higher initial coulombic efficiency (∼55%). More importantly, this carbon nanofibres web also exhibited excellent rate performance with considerably higher specific capacities at higher current densities (358 mAh g^{-1} at 1C). This superior electrochemical performance, in particular at high current rates, can be attributed to small lithium ion diffusion length and resilience in entangled carbon nanofibres to accommodate volume changes during charging and discharging.

Keywords. SU-8 photoresist; electrospun carbon nanofibres; anodes; high rate; lithium ion battery.

1. Introduction

Carbon nanofibres (CNF), due to their advantages like large surface area and thus enhanced interface of electrolyte and active material surface, short Li ion transport distances and high resilience to volume expansion during cycling even at high current densities, have drawn a great attention for being used as anode materials for lithium (Li) ion battery in recent years. Most of these studies available on the use of CNF as anode materials focus on vapour-grown CNF due to their enhanced conductivity and higher specific intercalation capacities compared with electrospun CNF [1,2].

Nanofibres can be synthesized by various methods like electrospinning, chemical vapour deposition (CVD), self-assembly and melt blowing [3–6]. Among these techniques, electrospinning appears to be a promising and scalable method for preparing continuous nanofibres. Electrospinning received much attention in recent years due to spinnability of a wide range of polymer materials, tunable fibre diameter and ability to make core–shell and composite nanofibres with varying surface morphology [7–10].

Even among a wide variety of electrospun fibres, only a few with better carbon yield such as those obtained from polyacrylonitrile (PAN) and polyvinyl alcohol derived CNF and their composites have been explored as anode material for Li ion battery [7,10,11].

In this work, we have used SU-8, an epoxy-based negative photoresist, as a precursor to CNF. SU-8 photoresist is widely used in microelectromechanical systems (MEMS) and it has been shown that SU-8-derived carbon thin films on stainless-steel (SS) collector can also be intercalated reversibly with Li ions with a significant capacity of 400 mAh g^{-1} (more than the theoretical capacity of graphite, 372 mAh g^{-1}) [12]. Further, we have also shown that SU-8 can not only be electrospun into nanofibres but also it can be micropatterned using lithography to fabricate three-dimensional micro-patterned arrays of nanofibres [13,14]. However, electrochemical performance of SU-8-derived electrospun CNF is still not studied, which is the aim of the present work. Integration of SU-8-based three-dimensional micro-electrode arrays with CNF may pave the way for the fabrication of high-surface-area hierarchical MEMS and NEMS structure with potential application in energy storage devices and as sensing platforms.

2. Experimental

2.1 *Materials*

SU-8 2015 (MicroChem Crop., USA), SS substrates (MTI Corp., USA), lithium foil (99.9% pure, Sigma Aldrich), glass microfibre filters (Whatman) and LP-30 electrolyte (1 M solution of $LiPF_6$ in a 1:1 v/v mixture of ethylene carbonate and diethyl carbonate) from Merck were used as received.

2.2 *Electrode preparation*

SU-8 2015 was electrospun in the form of nanofibres (electric field: 2 kV cm^{-1}, flow rate: 3 µl min^{-1}) over SS foil

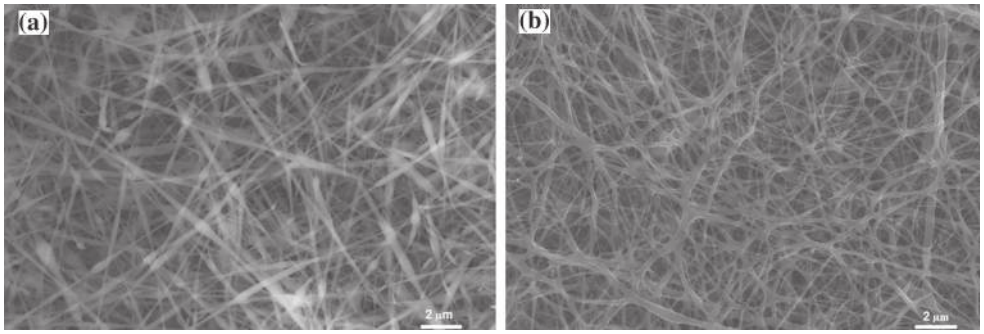

Figure 1. SEM image of electrospun SU-8 nanofibres (**a**) before pyrolysis and (**b**) after pyrolysis at 900°C.

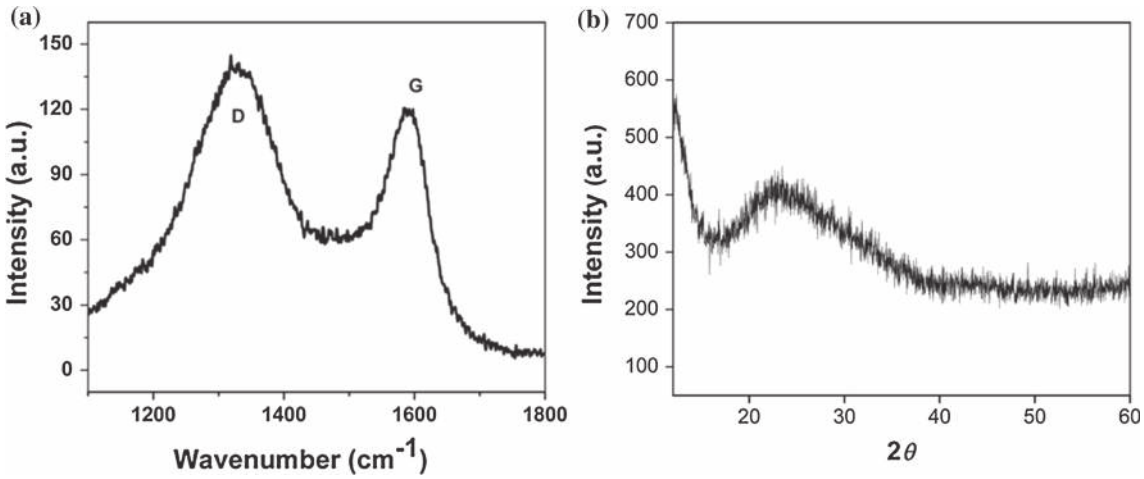

Figure 2. (**a**) Raman spectrum and (**b**) X-ray diffraction of SU-8-derived CNF pyrolysed at 900°C.

used as a current collector for 4 h. Thus deposited photoresist fibre webs were degassed for 30 min in a vacuum desiccator to remove excess solvent to prevent deformation of fibre morphology during soft baking. As-spun electrospun SU-8 photoresist nanofibres were then exposed to UV light to simulate photo-initiators, which helped in crosslinking the polymer chains in SU-8, followed by post-baking at 95°C for 15 min to complete the crosslinking. Further, these crosslinked fibre samples were hard baked at 150°C to relieve internal stresses built during the UV exposure and post-baking due to crosslinking of polymer. These crosslinked SU-8 nanofibres were pyrolysed using a controlled two-step pyrolysis process similar to SU-8-derived thin film pyrolysis to yield CNF [12].

3. Results and discussion

3.1 *Surface morphology*

Figure 1a and b shows the field emission scanning electron microscope (SUPRA 40, Zeiss) images of SU-8 electrospun fibres before and after pyrolysis, respectively. Although after pyrolysis, a significant shrinkage in average fibre diameter from 345.1 ± 71.3 to 231.8 ± 45.5 nm was observed, fibres morphology remained intact. This entangled nanofibre morphology of CNF, as shown in figure 1, allows maximum diffusion of Li ions due to intra-fibre porosity in entangled structures and the submicron fibre diameter.

3.2 *Structural characterization*

Raman spectrum of CNF shown in figure 2a was recorded with a 532 nm laser on a Bruker Raman microscope (Model: Senterra). Two prominent bands can be observed in both the samples, known as D and G bands. The D band (1335 cm^{-1}) corresponds to disorder and tetrahedrally bonded carbon, while the G band (1595 cm^{-1}) corresponds to the graphitic content and in-planar vibrations of graphene layers [15]. From the spectrum, I_D/I_G ratio and in-planar crystallite width were calculated as 1.18 and 3.55 nm, respectively [16], which reveal the glassy nature of the prepared CNF. Further, the X-ray diffraction pattern shown in figure 2b confirms the disordered nature of carbon. The broadness of the peak near 26°, which

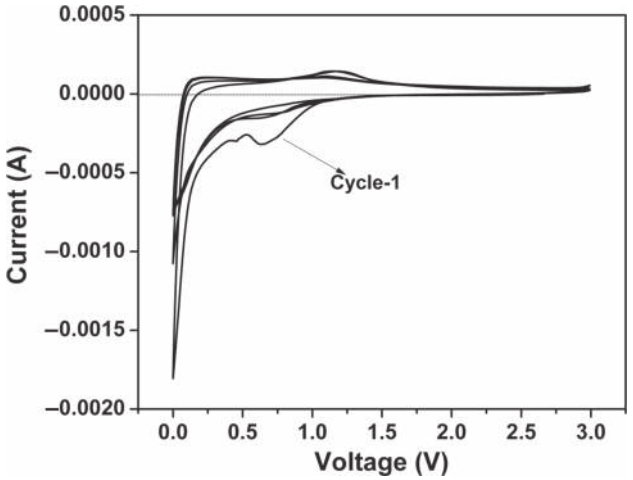

Figure 3. Cyclic voltammogram of SU-8-derived CNF at 0.1 mV scan rate.

corresponds to (0 0 2) plane, can be attributed to poor stacking of graphene layers in (0 0 2) plane.

3.3 *Electrochemical performance*

Electrochemical performance for SU-8-derived CNF was studied using a Swagelok cell packed inside a glove box; cell packing is described in detail elsewhere [17]. A glass microfibre filter soaked with LP-30 electrolyte was used as a separator. The cyclic voltammogram shown figure 3 was recorded at 0.1 mV s^{-1} between 0 and 3 V to investigate the electrochemical reactions taking place during cycling. The broad cathodic peak at about ∼0.5 V and sharp peak at 0 V correspond to solid electrolyte interface (SEI) formation on CNF electrode due to decomposition of electrolyte below 0.5 V and Li ion intercalation into carbon fibres, respectively [18]. There is an anodic peak in anodic scan near 1 V, which corresponds to desorption of Li from the surface of CNF. However, the cathodic peak corresponding to solid electrolyte formation disappears in subsequent cycles and there is no anodic reversible peak corresponding to the cathodic peak near 0.5 V, confirming the irreversible nature of SEI layer.

To analyse different contributions to the total electrode impedance, we have recorded electrochemical impedance spectra (Nyquist plot) in the frequency range of 10 mHz–100 kHz with 10 mV perturbation. Figure 4a and b shows the Nyquist plots of half-cells at open circuit voltage and after cycling, respectively. A semicircle in high-frequency regions followed by sharp increase in the imaginary part of the impedance in low-frequency range can be observed in both the figures. Contributions from external cell connections, solution resistance and conductions between active material and current collector at the interface appear in the high-frequency range. The small change in high-frequency region after cycling can be attributed to stability of the current collector and active material interface during the cycling. After cycling, semicircle diameter increased significantly and it can be attributed to increased polarization resistance due to formation of SEI on nanofibrous electrode surface due to electrolyte decomposition near 0 V as observed in cyclic voltammetry [19]. This change in charge transfer resistance due to SEI formation results in capacity fading at low C-rate cycling.

Galvanostatic charge–discharge experiments were carried out for 100 cycles at 0.1C as shown in figure 5a. Parallel to cycling at 0.1C rate, charge–discharge experiments at higher C-rates for 10 cycles each with freshly packed cell were also performed and specific capacity values are summarized in figure 5b. Initially, at 0.1C, first-cycle insertion and reversible capacity were measured, respectively,

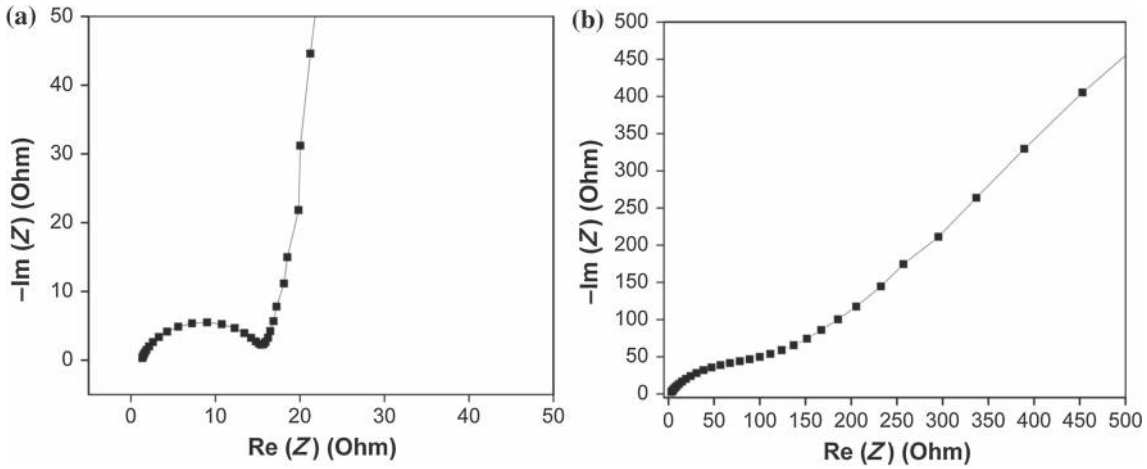

Figure 4. Nyquist plot showing the experimental data (**a**) before charge–discharge experiments at open circuit voltage and (**b**) after 10 charge–discharge cycles.

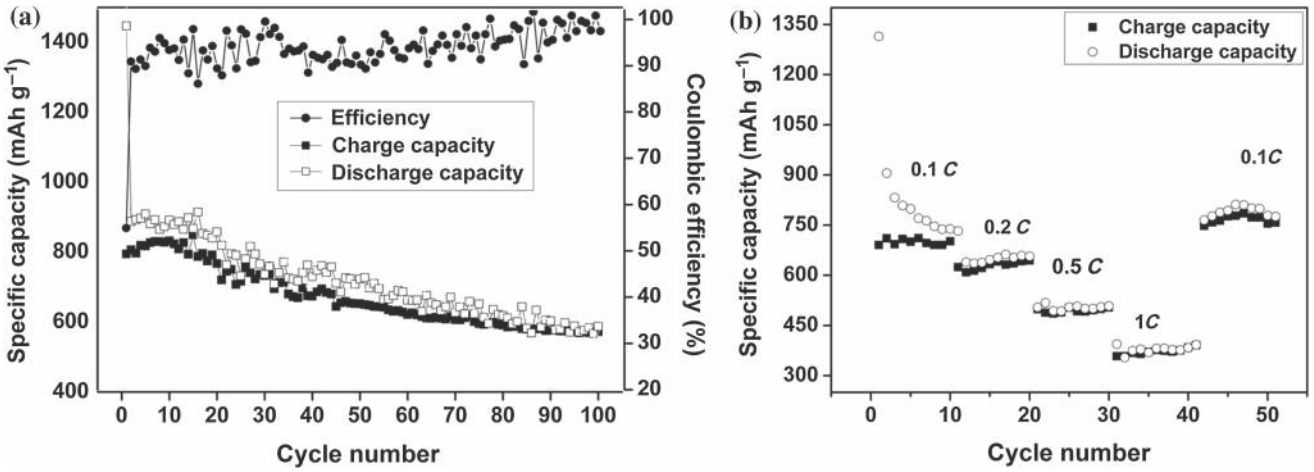

Figure 5. (**a**) Cyclic performance at $0.1C$ for 100 cycles and (**b**) rate performance at 0.1, 0.2, 0.5 and $1C$ of SU-8-derived CNF.

Table 1. Summary of cyclic performance and capacities for SU-8-derived CNF as anode at different C-rates.

C-rate	Discharge capacity (mAh g^{-1})	Charge capacity (mAh g^{-1})	Initial efficiency (%)	Efficiency after 10 cycles (%)	Charge capacity after 10 cycles
$0.1C$	1314.4	690.6	52.5	95	701.8
$0.2C$	732.5	624.4	85.2	98.1	644.4
$0.5C$	504.4	498.7	98.8	99.1	503.7
$1C$	394.4	358.1	90.8	100	384.3

as 1447 and 795 mAh g^{-1} with significantly higher initial coulombic efficiency of 54.9%. These values are considerably higher than those of not only SU-8-derived carbon films ($\sim$400 mAh g^{-1} at $0.1C$) but also most widely used PAN- and other polymer-precursor-derived electrospun CNF [7,10,11]. For cyclic stability, we measured the specific intercalation capacity after 100 cycles, which was found to be stable at 572 mAh g^{-1} with coulombic efficiency of 98% at $0.1C$ rate.

Impressively, at higher C-rates, specific reversible capacities values for SU-8-derived CNF were reported to be $630 \pm 12, 495 \pm 6$ and 374 ± 9 mAh g^{-1} for 0.2, 0.5 and $1C$, respectively. Table 1 shows a summary of the cyclic performance in terms of specific capacity and coulombic efficiency at different current densities. Minimal capacity fading and improved coulombic efficiency can be observed at higher C-rates (90.8% at $1C$ rate). This enhanced specific capacity and rate performance for SU-8-derived carbon nanofibres web can be attributed to entangled nanofibres morphology with glassy microstructure with more number of nanopores due to random alignment of small graphene layers, which helps in adsorption of Li over edge planes and nanopores formed by randomly arranged graphene layers [20].

4. Conclusions

In summary, CNF synthesized by controlled pyrolysis of electrospun SU-8 nanofibres exhibited superior electrochemical performance than any other polymer-precursor-derived CNF ever reported in literature. Further, as compared with SU-8-derived carbon thin films, CNF web showed not only nearly double specific reversible capacity at $0.1C$ but also superior intercalation capacity at higher rates ($1C$). Furthermore, these photoresist-derived CNF showed excellent cyclic performance at higher C-rates; e.g., specific capacity values at $1C$ are close to carbon thin films specific capacity at 10 times lower current density ($0.1C$). This exceptional performance of photoresist-derived electrospun CNF can be attributed to adsorption of Li-ions over edge planes of small crystallites and nanopores in glassy CNF at low C-rates, while at higher C-rates, short diffusion length in fibres and tolerance of expansion and shrinkage during faster Li insertion and de-insertion play a key role. The use of photoresist provides the possibility of fabricating three-dimensional arrays of CNF-based electrodes using photolithography within the same footprint area to enhance the energy density for Li ion battery further.

Acknowledgements

We acknowledge the Indian Institute of Technology, Hyderabad, for providing necessary research infrastructure to carry out this work. CSS acknowledges the DST INSPIRE faculty award research grant.

References

[1] Subramanian V, Zhu H and Wei B 2006 *J. Phys. Chem. B* **110** 7178
[2] Candelaria S L, Shao Y, Zhou W, Li X, Xiao J, Zhang J G *et al* 2012 *Nano Energy* **1** 195
[3] Li C, Yin X, Chen L, Li Q and Wang T 2009 *J. Phys. Chem. C* **113** 13438
[4] Lee J K, Wan K, Ju J B, Cho B W, Cho II W, Park D *et al* 2001 *Carbon* **39** 1299
[5] Wang Y, Zheng M, Lu H, Feng S, Ji G and Cao J 2010 *Nanoscale Res. Lett.* **5** 913
[6] Ellison C J, Phatak A, Giles D W, Macosko C W and Bates F S 2007 *Polymer* **48** 3306
[7] Ji L, Yao Y, Toprakci O, Lin Z, Liang Y, Shi Q *et al* 2010 *J. Power Sources* **195** 2050
[8] Ji L and Zhang X 2009 *Carbon* **47** 3219
[9] Thompson C J, Chase G G, Yarin A L and Reneker D H 2007 *Polymer* **48** 6913
[10] Liu B, Yu Y, Chang J, Yang X, Wu D and Yang X 2011 *Electrochem. Commun.* **13** 558
[11] Mao X, Hatton T A and Rutledge G C 2013 *Curr. Org. Chem.* **17** 1390
[12] Kakunuri M and Sharma C S 2015 *ECS Trans.* **66** 56
[13] Sharma C S, Vasita R, Upadhyay D K, Sharma A and Katti D S 2010 *Ind. Eng. Chem. Res.* **49** 2731
[14] Sharma C S, Sharma A and Madou M 2010 *Langmuir* **26** 2218
[15] Tuinstra F and Koenig J L 1970 *J. Chem. Phys.* **53** 1126
[16] Jawhari T, Roid A and Casado J 1995 *Carbon* **33** 1561
[17] Kakunuri M and Sharma C S 2015 *Electrochim. Acta* **180** 353
[18] Zhang S, Ding M S, Xu K, Allen J and Jow T R 2001 *Electrochem. Solid-State Lett.* **4** A206
[19] Ruffo R, Hong S S, Chan C K, Huggins R A and Cui Y 2009 *J. Phys. Chem. C* **113** 11390
[20] Liu Y, Xue J S, Zheng T and Dahn J R 1996 *Carbon* **34** 193